Shear-wave amplitude anomalies in south-central Wyoming

ROBERT R. KENDALL
Amoco Production

J-MICHAEL KENDALL
University of Leeds

Amoco recently acquired four surface-seismic shear-wave lines, four multicomponent VSP's and three crossed-dipole sonic logs in south-central Wyoming. A feature of this region is that areas of increased gas production correlate with areas of increased fracturing. After seismic processing of the shear-wave lines, it was observed that reductions in the relative amplitude of the slow shear-wave (S2) seismic section with respect to the fast shear-wave (S1) section correlate with areas of greater gas production. These amplitude anomalies are attributed to anisotropy due to the preferential alignment of vertical fractures where S1 is polarized parallel to the fracture azimuth and S2 is polarized perpendicular to the fractures. Furthermore, preferred directions of fast shear-wave polarization, and hence fracture strike, derived from crossed-dipole sonic logs and multicomponent VSPs are in agreement with the directions determined from the surface seismic. Modeling of wave propagation effects due to the anisotropy illustrates how enhanced open fracturing may cause shear-wave amplitude anomalies. Seismic waveforms are sensitive to the fracture density and orientation and the nature of the material within the fractures. The modelling also shows that the range of offsets used in stacking shear-wave data must be carefully selected. Locations of polarity reversals and the onset of critical reflections can vary dramatically with fracturing.

Introduction. Evidence of anisotropy in fractured hydrocarbon reservoirs has the potential to be a powerful interpretation tool for characterizing the intensity and orientation of fractures. The presence of these fractures can dramatically improve production rates, most notably in tight formations. Amoco has acquired, processed and interpreted the pure shear-wave components of four 9-component (9-C) seismic lines that were acquired in south-central Wyoming (Figure 1). Additionally, crossed-dipole sonic logs and multicomponent VSPs have been acquired, processed and interpreted.

The zone of interest, at approximately 3 100 m, is a mostly shale-dominated sequence with interbedded sandstone layers that are roughly 10 m thick. Deposition of the sandstone (offshore barrier bar) represents a short-lived regressive pulse within a more dominant transgressive system. The reservoir is primarily gas filled and analysis of drill core has shown strong regional variations in the degree of fracturing within these reservoirs.

A medium with preferentially aligned vertical fractures will exhibit azimuthal anisotropy (Crampin, 1984, *Geophysical Journal of the Royal Astronomical Society).* The fast shear-wave will be polarized parallel to the crack faces, while the slower shear-wave is polarized orthogonal to the crack faces. Fracture orientation within the sandstone was determined from the fast shear-wave polarization direction using the Alford technique. A layer stripping technique (Thomsen et al., "Layer stripping for azimuthal anisotropy of reflection seismic data," in publication) was used to verify that the preferred direction was constant (N45°E ± 15°) with depth. These rotation angles were confirmed through the interpretation of the crossed-dipole data and multicomponent VSPs (N60°E ± 15°). Evidence of fracturing was inferred from variations in amplitude strength between the fast and slow shear-wave components using a method suggested by Thomsen ("Reflection seismology over azimuthally anisotropic media," GEOPHYSICS, 1995) and applied by Mueller ("Prediction of lateral variability in fracture intensity using multicomponent shear-wave surface seismic as a precursor to horizontal drilling in the Austin chalk," *Geophysical Journal International).* Here we find that shear-wave amplitude anomalies (SWAA) coincide with production anomalies that are an order of magnitude more productive than production in the surrounding regions. Drilling has confirmed the interpreted fracture azimuth (core measurements show that the fractures strike N60°E).

In order to better interpret the data,

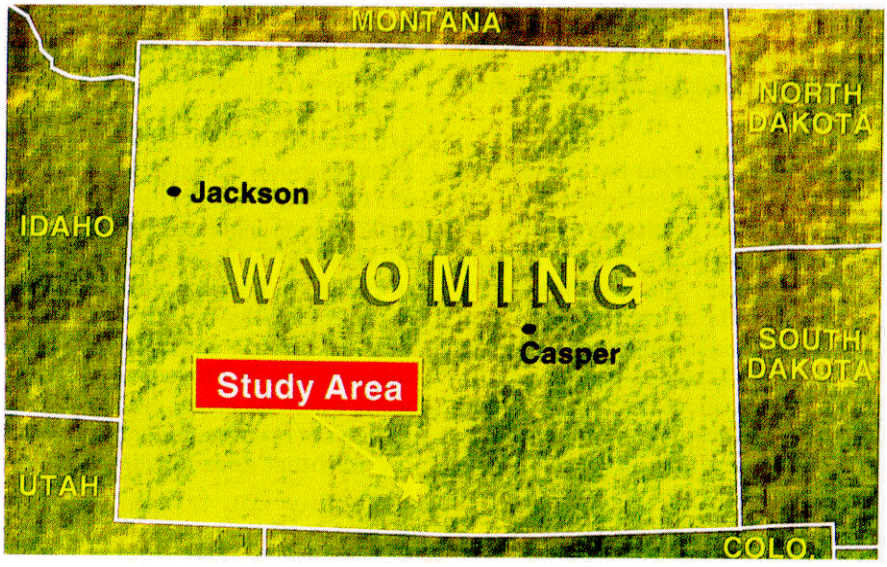

Figure 1. General location of our study area.

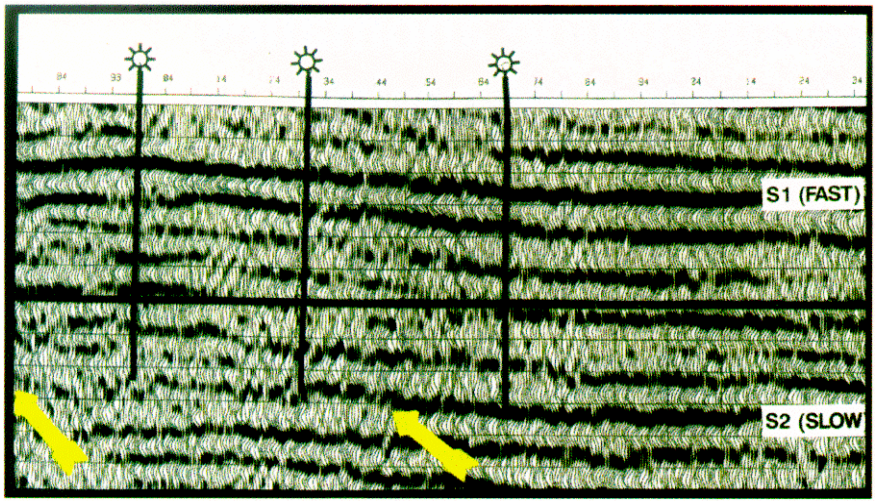

Figure 2. Final rotated shear-wave sections. The upper section is the fast or S1 section while the lower is the slower or S2 section. Note the amplitude reduction on the slower section at the identified level towards the left of the section (between arrows). Production coming from the zone located between the arrows is an order of magnitude greater than the surrounding regions.

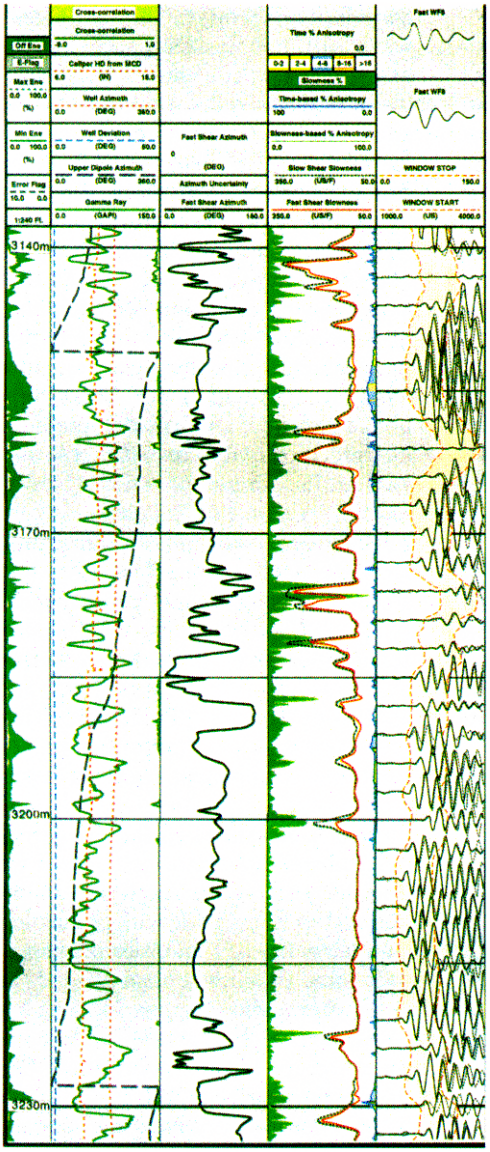

Figure 3. A typical cross-dipole sonic log from the study area. From left to right the five tracks are: (1) the minimum and maximum off-diagonal shear-wave energy and depth. Areas of greatest anisotropy occur where there is the greatest separation between the maximum and minimum curves (areas with a lot of green filling); (2) the gamma-ray log, well azimuth, well deviation and well diameter (caliper); (3) the azimuth of the fast shear-wave polarization; (4) the slownesses of the fast and slow shear-waves and slowness-based and interval-transit-time-based percentage anisotropy (see color scale at top); (5) the fast and slow shear-waveforms for one receiver pair and the analysis window (dashed lines).

we have modeled the seismic response of reflections from an anisotropic sandstone layer with preferentially aligned fluid and gas filled cracks. The modeling results confirm the interpretation of the amplitude anomalies on the surface seismic and also reveal some of the subtle variations that may occur due to variations in fracture intensity, crack aspect ratio and crack fill material.

Data analysis. This involves three types of data: shear-wave surface seismic; crossed dipole sonic log; and multicomponent VSP.

Shear-wave surface seismic. These data were acquired using four horizontal motion vibrators (Amoco's rotating baseplate Mertz 18's). The signal to noise ratio (S/N) was improved by running the vibrators in a box pattern, as opposed to an in-line configuration. It was also observed that using more short sweeps, as opposed to fewer long ones, improved the S/N. The optimal sweep turned out to be 6-36 Hz, linear over 16 seconds, with a 7 s record length. Group and shot intervals were 37 m, with the shots between the groups. An SGR recording system was used to record the 660 channels, producing a far offset of 4000 m in a split-spread configuration. 1 lo-fold coverage was achieved.

These data were processed using a true amplitude approach, since we were ultimately interested in comparing amplitudes on the fast (S1) and slow (S2) sections. Refraction statics were calculated on the pure cross-line component, due to the minimal P-wave first arrival energy on these records, and that solution was then applied to each of the four components. Residual statics were calculated and applied independently for each component. Velocity analysis, as with P-wave processing, was crucial and an average velocity function for the four components was used for normal-moveout (NMO) corrections. The data were stacked by limiting the angle of incidence to less than 30" (angle stack), thus ensuring that only precritical arrivals were used (see modeling section). A Radon filter proved to be very effective for removing most of the coherent noise that often dominated the data. Finally, we applied Alford rotation analysis to determine the preferred directions and the data were then rotated to that angle for the amplitude analysis. Figure 2 shows the data quality as well as a typical SWAA. For this line, the optimal rotation angle suggested a fracture strike of N45°E. Three wells are marked in Figure 2. Two are above a SWAA anomaly (between the arrows on the left side of Figure 2) and one is not (right side of Figure 2). production in the two wells which lie above the SWAA was an order of magnitude more than that in the well that does not lie above the SWAA.

Crossed-dipole sonic log. Crossed-dipole data were acquired and processed

in order to resolve detailed variations in azimuthal anisotropy. Figure 3 shows a representative crossed-dipole sonic log from this area. In the interval between depths of 3140.3230 m, there is predominantly one preferred direction at N60°E. However, the crossed-dipole log is sensitive enough to detect minor (<1 m) variations in azimuthal anisotropy with depth. The majority of scatter in the measured azimuth can be attributed to zones of isotropy or to areas of poor data quality. The off-diagonal energy curves (minimum is on the left and maximum is on the right on track 1) help identify these regions. The maximum off-diagonal energy curve does not separate from the minimum off-diagonal energy curve in the more isotropic areas and the minimum off-diagonal curve does not return to zero in the noisier regions. Large values of anisotropy are seen in the less noisy areas where the energy curves are well separated. This is indicated on the anisotropy curves (track 4) and by the differences in the fast and slow shear-waveform arrivals (track 5).

It is observed that the N60°E azimuth is most stable in the sandstone zones (gamma ray is track 2) with high degrees of fracture induced anisotropy. The more shaley surrounding zones show evidence of much weaker anisotropy. Within these zones a secondary fracture azimuth is also observed with an azimuth of N150°E. The thin more brittle sandstone beds are more likely to fracture than the surrounding more ductile shales. Given the historical tectonic complexity of this region it is not surprising to have more than one fracture azimuth.

Furthermore, it is not unusual to observe orthogonal fracture strikes in outcrop and in core (Nelson, 1985, Geologic analysis of naturally fractured reservoirs, ***Gulf Publishing Company).*** A geologic (both depositional and tectonic) explanation of the presence of orthogonal fracture sets is not within the scope of this paper. The cross-dipole sonic log can resolve variation in anisotropy on the scale of a few meters. The low-level anisotropy in the shales will not be resolvable in the comparatively long-wavelength VSP and surface-seismic data. Instead, the high-degree of anisotropy in the thin sandstone layers will dominate in the rotation analyses for the VSP and surface seismic.

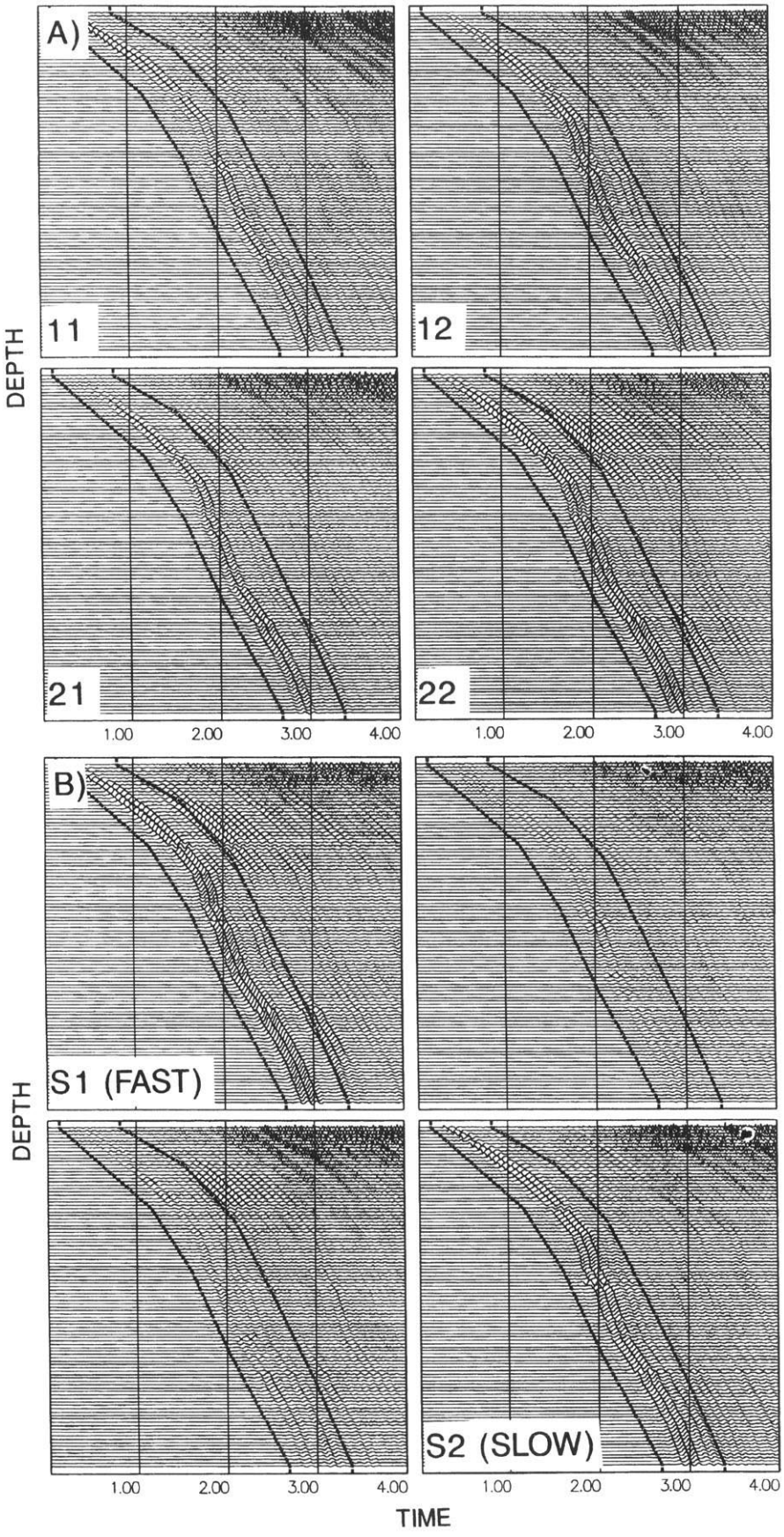

Figure 4. The four components of the VSP before (4a) and after (4b) Alford rotation into the direction of fast and slow shear-wave polarization.

Multicomponent VSP. Four wells in this area were used to acquire multicomponent VSPs. Azimuthal-anisotropy analyses using Alford rotations and fast and slow shear-wave arrival time differences (time-delay) were used to characterize the anisotropy. Figure 4 (a, b) shows the four components of the VSP data from one well before and after rotation. Clearly the S/N in these data is very high. The rotation analysis attempts to rotate the shear-wave data into the fast and slow polarization directions (main-diagonal components), thereby minimizing the energy on the off-diagonal components. The postrotation data (Figure 4b) show a good minimization of the first arrival amplitudes on the off-diagonal components, within the identified window, confirming our interpreted azimuth. Figure 5 (a, b) shows the polarization angle (azimuth) and time delay respectively. The rotation analyses and time-delay analyses of these data was done using the EAP software SWAP (Li and Crampin, GEOPHYSICS, 1991). SWAP also has the functionality to do Winterstein (Winterstein and Meadows, SEG *Expanded Abstracts*, 1990) layer stripping to isolate variations in anisotropy with depth. These data showed a consistant fast-shear-wave azimuth with depth.

The polarization angle N60°E (Figure 5a) is consistent with depth. There is some scatter in the azimuth, most notably in the shallower section (<1920 m). The time-delay curve can be broken down into 4 zones (Figure 5b). The majority of the traveltime delay (hence anisotropy) is accrued in the first zone, from 0- 1920 m. This zone includes the weathering, subweathering and generally less competent rock. Others (Kramer and Davis, 1992, TLE) have documented this shallow zone as being highly anisotropic. Zone 2 has been interpreted to be isotropic and extends to a depth of approximately 3 100 m. Zone 3 is between 3100 and 3360 m and includes the target interval. The percentage anisotropy in this zone is about 4% based on the time delay information on Figure 5b. This is in agreement with the 4-8% anisotropy that is observed for the fracture zones on the cross-dipole sonic log.

Summary of SWAA method. Figure 6 illustrates a fracture model that could create a SWAA. We consider two near-normal-incident reflections from two points (marked 1 and 2). The sandstone has a higher impedance than the overlying shale and we assume the shale is isotropic. The reflection coefficient for orthogonally polarized shear waves will be the same at location 1. That is, the shear wave polarized in the plane of the page (in-line) will have the same reflection coefficient as the shear wave polarized perpendicular to the plane of the page (crossline). In contrast, the reflection coefficients for the two orthogonally polarized shear waves will be different at location 2. The shear wave that is polarized in the in-line direction (perpendicular to the cracks) will detect a less rigid, therefore lower velocity, sandstone at location 2 than that detected by the shear wave that is polarized in the cross-line direction (parallel to the cracks). Therefore, the shear wave that is polarized in the cross-line direction will have a greater reflection coefficient (bigger amplitudes) than the shear wave that is polarized in the in-line direction. In the next section we show that crack intensity, crack aspect ratio and crack fill material all affect this decrease in amplitude. Furthermore, the polarization of the reflected shear- waves at location 2 will be af-

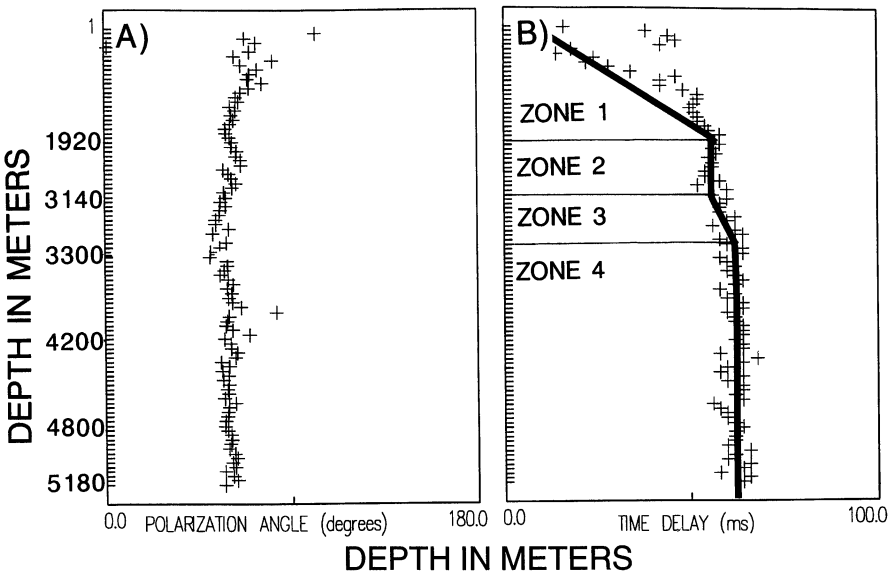

Figure 5. Fracture azimuth (5a) and time delay (5b) as determined using the program SWAP, Note the two predominant zones (1 and 3) of increased time-delay which indicates anisotropy and the more-or-less depth consistent azimuth that is clustered around N60°E.

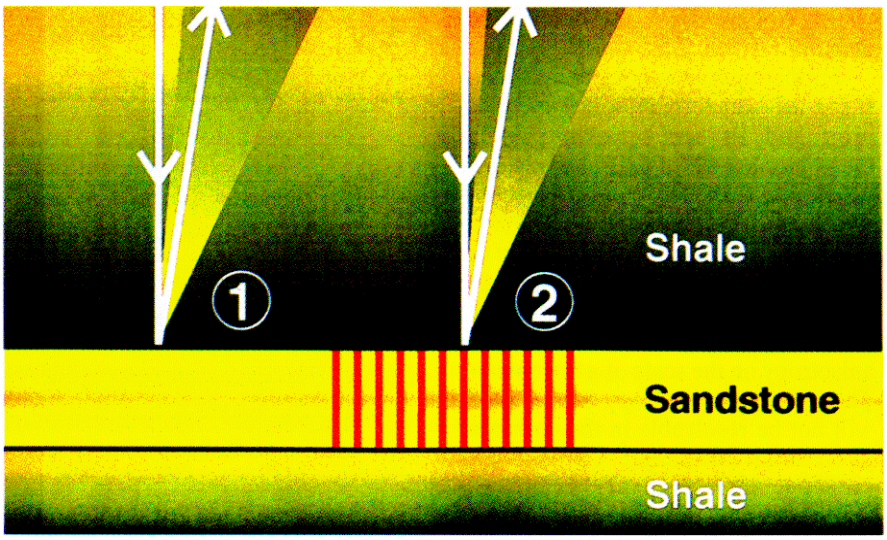

Figure 6. Schematic diagram of a fracture model which could generate the observed shear-wave amplitude anomaly. Note that the ray propagates in a solely isotropic media. For rays that propagate into the fractured region, we refer to the in-line and cross-line polarizations as S2 and S1.

fected by the strike of the fractures, regardless of the source polarization. It is perhaps appropriate to refer to the rotated sections as S1 and S2, even though the waves propagate entirely through an isotropic medium, since the shear-wave polarizations are affected by the fracture strike.

Figure 2 shows an example of this amplitude difference on a seismic section while Figure 7 illustrates the amplitude difference using an amplitude extraction technique. The reflector is labeled consistently on both figures as S 1 and S2. Since the bed thickness is extremely small compared to the total depth, traveltime differences between S1 and S2 accrued in the anisotropic thin-bed will be below the resolution of the seismic data. In contrast, the amplitude extraction technique is very sensitive to the anisotropy, even with these noisy data and the thin beds (Figures 2 and 7). In other words, the amplitude technique (using SWAAs) has better vertical resolution than do traveltime methods.

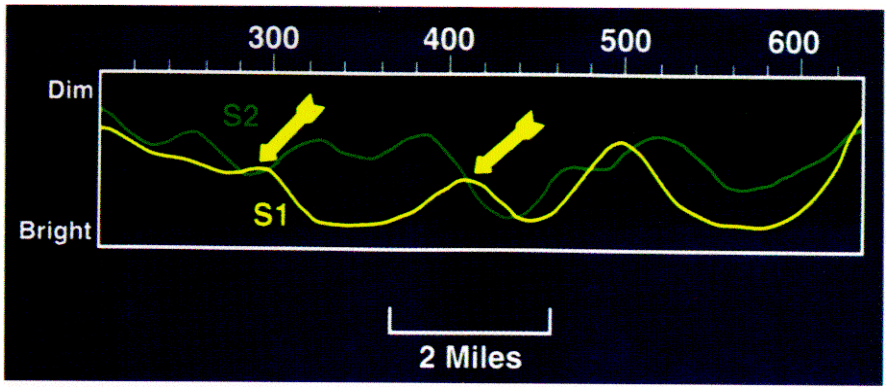

Figure 7. Extracted amplitudes as identified on Figure 2. The arrows indicate the region between which the anomaly, that is identified on Figure 2, is located.

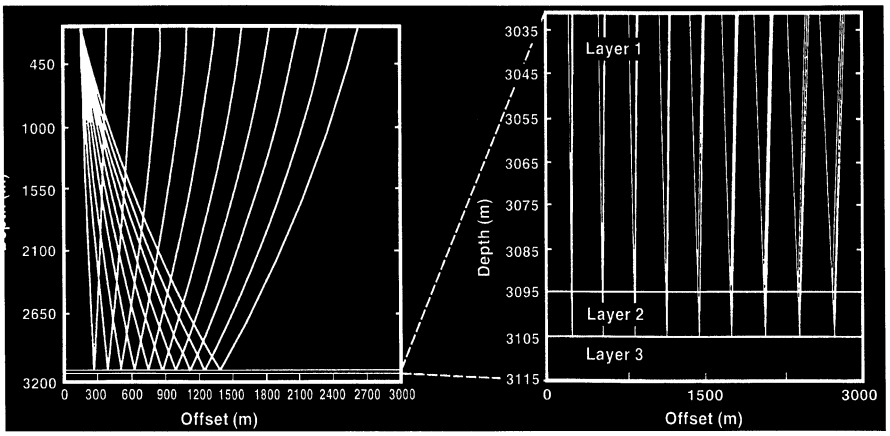

Figure 8. Shear wave raypaths through the model of a thin fractured (anisotropic) sandstone layer embedded in an isotropic background medium. Note the splitting of rays at further offsets as they reflect from the top and bottom of the anisotropic layer.

Modeling. In order to interpret the SWAAs in terms of fracture intensity and orientation, one must first understand the nature of wave propagation in such anisotropic structures. Modeling of these data has been done with a ray-based program (ATRAK) which handles general anisotropy, 3-D structure and nonplanar layers (Guest and Kendall, 1993, *Canadian Journal of Exploration Geophysics).* Our results show that the anisotropy can significantly affect the shear-wave amplitudes. Furthermore, the locations of critical points and nulls in reflection coefficients are very sensitive to the nature of the anisotropy. Our model, which is based on well results, has a thin (10 m) anisotropic layer which starts at a depth of 3095 m (Figure 8). The anisotropy is due to the preferential alignment of thin cracks within an otherwise isotropic sandstone. For simplicity, we have assumed that the surrounding rock is isotropic and has a linear velocity gradient with depth. Any anisotropy within the surrounding shales has been neglected. It is assumed that the fractured sandstone exhibits azimuthal anisotropy (hexagonal symmetry) with the (horizontal) symmetry axis oriented in the in-line direction (the fractures are striking in the cross-line direction).

We adopt the approach of Hudson ("Overall properties of a cracked solid," *Mathematical Proceedings of the Cambridge Philosophical Society,* 1980) to estimate effective elastic constants of the fractured sandstone. Hudson's expressions are accurate to second order in crack density, but this theory does not account for the effect of the cracks being hydraulically interconnected. Estimates of the fracture attributes for our area of study have been obtained from geologic analyses of drill core. The degree of fracturing, which partially controls production in this area, is highly variable. As end-member models we consider cases where the fracturing varies from extreme to nonexistent (isotropic) and cases where the fractures are gas filled and fluid filled. For the fractured cases we consider a fracture density of 0.15 and a crack aspect ratio of 0.00001, estimates of which were obtained from drill core.

It is instructive to first inspect the slowness and velocity surfaces for the range of anisotropy we are considering (Figure 9). Figure 9a corresponds to the case for a wave propagating in the isotropic sandstone (not fractured) at location 1 in Figure 6. Figure 9 (b, c) corresponds to plausible wavefronts in the anisotropic sandstone (fractured) at location 2. Note that these wavefronts are spherical for the isotropic case but not for the anisotropic case and that two quasi-orthogonally polarized shear-waves will propagate in the anisotropic region. For wave propagation in the vertical direction (x3), the fracturing has little effect on the qP-wave and transversely-polarized shear-waves (S1 or cross-line shear-wave). Recall that according to our model, the S1 waves are polarized parallel to the fractures. On the other hand, the radially-polarized S2 or in-line shear-waves (those waves polarized perpendicular to the fractures) are much slower in the vertical direction. For wave propagation along the symmetry direction (x 1), both shear waves propagate with the same velocity and are slow relative to the isotropic case. The qP-waves in this direction are

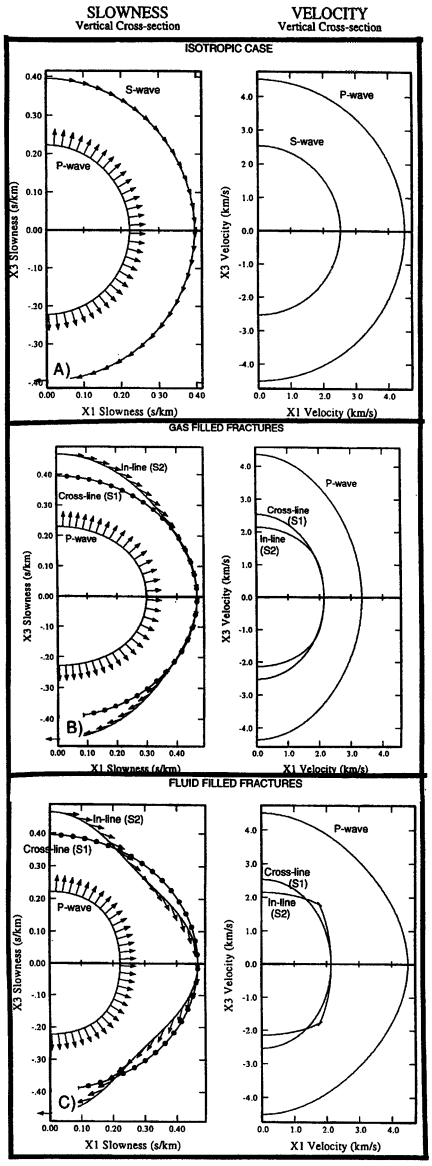

Figure 9. Vertical sections of the slowness surfaces and polarizations (LHS) and wave (group velocity) surfaces (RHS) for a medium with vertically aligned fractures with crack-face normals oriented along the x 1 axis. The fracture density is 0.15 and the crack aspect ration is 0.00001. (a) No fracturing (isotropic); (b) gas filled cracks; (c) fluid filled cracks.

much slower for the gas-filled case than the fluid-filled case (compare Figures 9b and Sc). Our numerical experiments show that the variation in S l-wave (cross-line) velocity from vertical to horizontal propagation directions is not very sensitive to the crack aspect-ratio or the inclusion material. In contrast the S2-wave (in-line) is very sensitive to these parameters.

Wavefront folding, or triplications, will develop as the cracks become "skinnier." The fluid-filled cracks are more sensitive to this than the gas-filled cracks.

Figure 10 (a, b, c) shows synthetic S-wave seismograms for reflections from the top of the thin sandstone layer. In keeping with the actual field recording, waveforms are modeled for offsets out to ~ 4 km. A 20 Hz Ricker wavelet is used. Despite traveling solely through isotropic media the waveforms are very sensitive to anisotropy in the underlying sandstone layer. This is due to polarity dependent variations in the velocity contrast across the isotropic/anisotropic interface. In the isotropic case the S-velocity increase across the interface is from 2000 m/s to 2530 m/s. Figure 10a shows that for near-normal-incidence the cross-line and in-line amplitudes are equal in the isotropic case as expected. There is a null in the in-line reflection coefficient for offsets near 1600 m while there is one near 3 100 m, near the critical angle, for the cross-line case. Figure 10 (b, c) shows the waveforms for the anisotropic cases (gas and fluid filled cracks respectively). The cross-line waveforms for near vertical arrivals are essentially the same as those for the isotropic case. In contrast, the in-line amplitudes are roughly half those of the cross-line case. This is due to the diminished velocity contrast across the interface due to the aligned fractures.

Waveform variations with offset for the anisotropic cases are quite different from those for the isotropic case. In comparison, the point of critical reflection for the cross-line-waveforms is moved to further offsets because the cross-line velocities decrease in the anisotropic layer with increasing angle of incidence on the boundary. This is apparent on the wave surfaces if one considers variations in wave propagation in the region between the x 3 and x 1 directions (Figure 9). The in-line waveforms are sensitive to the nature of the crack fill material. In comparison to the isotropic case, the null in reflections for the gas-filled case is at further offsets while the null for the fluid filled case is at nearer offsets. At far offsets the amplitudes for the gas-filled case are much smaller than those for the other cases. The in-line amplitudes for the fluid-filled case are almost as high as those for the isotropic case. This is due to the high velocities near the emerging triplication on the wave surfaces in the region 45° from the vertical (Figure 9c). In contrast, the velocities

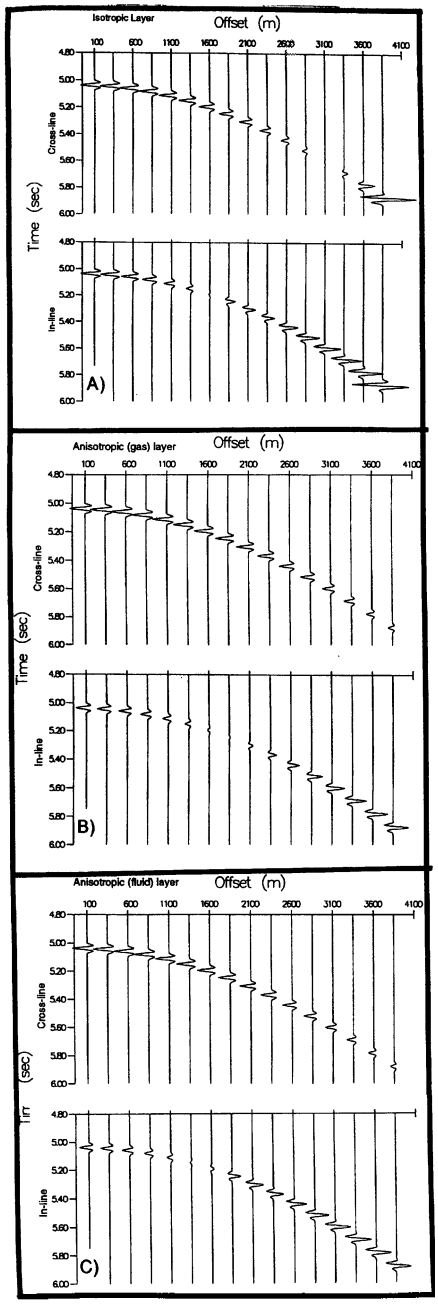

Figure 10. Synthetic S-wave seismograms for reflections from the top of the thin fractured sandstone layer modelled using the program ATRAK. The synthetics are generated using ray theory and a 20 Hz Ricker wavelet. The cross-line and in-line records are shown for: (a) no fracturing in the sandstone layer (isotropic); (b) gas filled cracks; (c) fluid filled cracks.

for the gas-filled case decrease smoothly towards the horizontal (Figure 9b). Our numerical experiments have also shown that this in-line waveform behavior at far offsets is also dependent on the crack aspect ratio.

Figure 11 (a, b, c) shows the com-

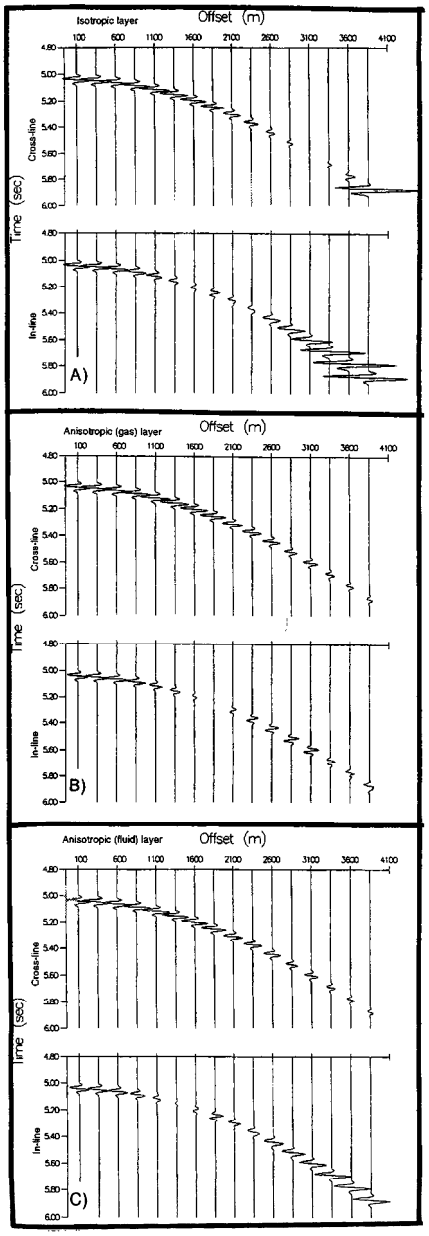

Figure 11. Synthetic S-wave seismograms for reflections from the top and bottom of the thin fractured sandstone layer. The synthetics are generated using ray theory and a 20 Hz Ricker wavelet. The cross-line and in-line records are shown for: (a) no fracturing in the sandstone layer (isotropic); (b) gas filled cracks; (c) the case of fluid filled cracks.

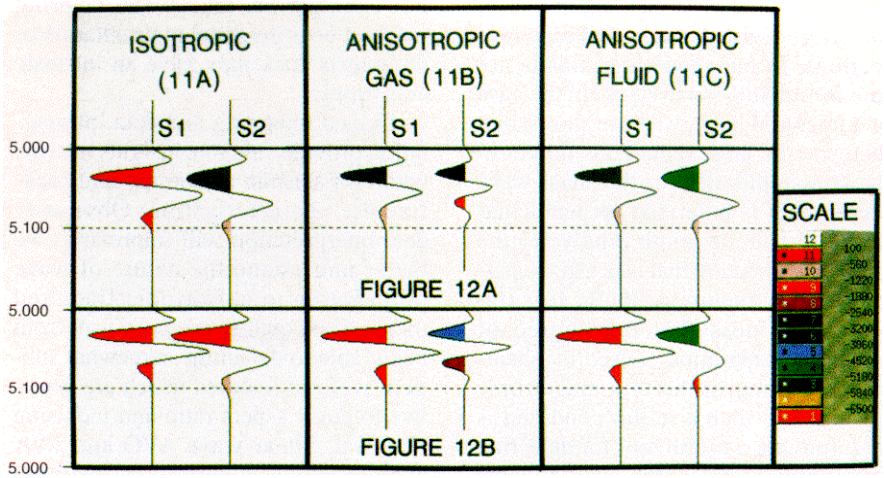

Figure 12. Stacks of the synthetic waveforms shown in Figure 11. (a) NMO corrected stacked traces using all of the traces (0–3850 m) for the cross-line (S1) and in-line (S2) records. (b) Range-limited stack using offsets equivalent to those used in the processing of the field data (0–3350 m). The color scale is linear and only the negative amplitudes get assigned a color. Note the more dramatic decreases in amplitudes, from S1 to S2, for the anisotropic cases than for the isotropic case. The full offset stack includes reflections that have gone postcritical; the amplitude differences on the full-range stacks are less obvious.

posite waveforms for reflections from both the top of the thin sandstone layer and the bottom of the layer. The layer is roughly l/10-wavelength in thickness so therefore seismically detectable, but there will be waveform interference effects. All of the features observed for the single reflection and discussed above are still apparent. The only notable difference is that the in-line shear-wave (S2) amplitudes for the gas-filled case are even weaker at the distant offsets. Traveltime measurement of shear-wave splitting is not a diagnostic tool for detecting fractures in such a thin layer. Not only is the degree of splitting minuscule, the reflections for the top and bottom of the layer are indistinguishable for the wavelengths we are dealing with. Instead reductions in reflection amplitudes are strongly indicative of the fracturing. This is in agreement with the observed field data and provides a plausible explanation (though nonunique) for the observed enhanced production within the regions of SWAAs.

The reflection data from Figure 11 (a, b, c) were NMO corrected and stacked (Figure 12a, b). Figure 12a shows the full-range stacks using all of the traces (o-3850 m) for the cross-line (S1) and in-line (S2) records. Figure 12b shows the range-limited stacks using offsets equivalent to those used in the processing of the field data (o-3350 m). The field data were angle-stacked using only angles of incidence less than 30". This corresponds roughly to offsets of 3350 m for a reflector at a depth of 3 100 m. The range-limited stacks show very clear SWAAs for both the gas- and fluid-filled fracture cases. The S2 amplitudes are roughly half the S1 amplitudes for the anisotropic models. In contrast, the S1 and S2 amplitudes are nearly the same for the isotropic case. The full-range stacks include the high-amplitude post-critical reflections at the farthest offsets. The difference between the fluid-filled case and the isotropic case is no longer so obvious. The gas-filled case still shows the S2 amplitudes to be much smaller than the Sl amplitudes. Only precritical reflections should be used in the stacks to avoid the more dominant high-amplitude and phase distorted postcritical reflections.

Conclusions. In our study area, lateral amplitude variations, as observed predominantly on the slow-shear (S2) seismic sections, correlate with areas of greater gas production. Furthermore, preferred directions of fracturing derived from measurements of anisotropy on crossed-dipole sonic logs and multicomponent VSPs are in agreement with face seismic. Anisotropic seismic modeling of these data illustrates that enhanced open fracturing may be causing the shear-wave amplitude anomalies.

Our waveform modeling has provided a qualitative explanation for the observed SWAAs in the data. The waveforms are very sensitive to the fracture density and orientation which is valuable information for a drilling program. For reflections from an isotropic layer embedded in an isotropic medium there is no difference between

the in-line and cross-line amplitudes in the range-limited stacked shear-wave sections. In our modelling, this is not true for the full-range stack. In the case of a fractured layer, we have shown that there can be large reductions in the reflection amplitudes for the shear-wave section that is polarized perpendicular to the fracture azimuth relative to the shear-wave section that is polarized parallel to the fracture azimuth. It is important to note that the degree of traveltime separation caused by shear-wave splitting in the thin anisotropic layer is less than a millisecond and is therefore not a useful tool for detecting anisotropy in such a thin layer. It is the waveform effects which are diagnostic of the anisotropy.

There are many interesting aspects of rock-fracture characterization that we have not addressed. The effects of hydraulically interconnected cracks and equant porosity (Thomsen, "Elastic anisotropy due to aligned cracks in porous rock," *Geophysical Prospecting,* 1995) will be explored in the future. We have also not considered the effects of more complicated elastic symmetries. For example the cracks and layering may not be orthogonal in orientation or the matrix rock may have an intrinsic anisotropy.

Linked modeling and data interpretation provide valuable insights into the nature of seismic anisotropy and rock-fracture characterization. Obviously data interpretation will improve as we better understand the nature of wave propagation in anisotropic fractured media. Data quality is a long way from being able to detect the somewhat subtle waveform features which are sensitive to crack aspect ratio and inclusion material. Shear-wave AVO and AVA analyses hold potential for obtaining such information. Finally, the application of these ideas to the 3-D domain will add further insights. LE

Acknowledgments. We thank Steve Clawson for providing the details of the core analysis and production histories, Mike Mueller, Leon Thomsen, and Sean Guest for constructive comments on the manuscript and Michele Simon for the editing of this issue. We also thank Amoco for allowing us to publish these results.

Robert R. Kendall received his bachelor's in geophysics from the University of Calgary in 1988 and his master's in geophysics from the Colorado School of Mines in 1992. He worked for Solid State Geophysical from 1988 to 1990 as a geophysicist and party manager. In 1992 he joined Amoco and now works in the seismic processing group (STAT).

J-Michael Kendall received his bachelor's and doctorate from Queen's University Kingston, Ontario in 1984 and 1991 respectively. He worked for Chevron Canada from 1984 to 1986. He was a postdoctoral fellow at Scripps Institution of Oceanography from 1992 to 1993 and was an assistant professor at the University of Toronto from 1993 to 1995. He is currently a university research fellow/lecturer at the University of Leeds in England.